ACS OMEGA

Open Access

http://pubs.acs.org/journal/acsodf

Article

Sensitive Electrochemical Immunosensor for Procymidone Detection Based on a Supramolecular Amplification Strategy

Qiushuang Ai, Xiren Yu, Yifan Dong, Li Zhang, Jingtian Liang, Dawen Zhang,* and Suyan Qiu*

Cite This: *ACS Omega* 2025, 10, 3108−3115

Read Online

ACCESS | Metrics & More | Article Recommendations | Supporting Information

ABSTRACT: A sensitive electrochemical immunosensor for procymidone detection was developed based on a supramolecular amplification strategy. β-Cyclodextrin (β-CD)-based nanomaterials were employed to immobilize ferrocene derivative (FC)-functionalized antibodies/antigens through host−guest interactions. With the presence of procymidone, the formed β-CD-labeled bioconjugates were immobilized on the antibody-modified electrode after the immunoreaction, indicating fabrication of the immunosensor. The FC/β-CD complexes were with multiplex electroactive species and provided more sites for recognition groups, resulting in signal amplification of the sensor. Monitored with differential pulse voltammetry, the proposed immunosensor exhibited a wide linear range from 5 pM to 0.1 μM with a low detection limit (LOD) of 1.67 pM. The as-prepared immunosensor possessed high sensitivity, specificity, and stability and showed great potential for monitoring procymidone in the field of food safety.

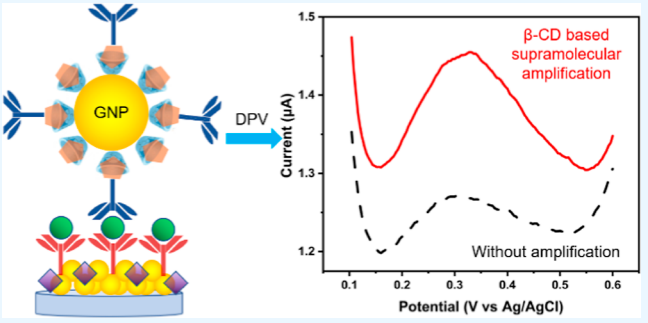

1. INTRODUCTION

As a fungicide pesticide, procymidone (PCD) has been worldwide used to prevent Sclerotinia sclerotiorum, gray mold, and black spot of vegetables, fruits, and crops.[1−3] Procymidone can accumulate in the human body through the food chain. Long-time and excessive exposure to PCD might cause organ deformities, lesions, and even cancer.[4−7] Considering PCD residues posing a threat to consumers, many countries have developed legislations to regulate and control PCD in agricultural products.

Conventional methods for PCD determination are traditional techniques such as gas chromatography−mass spectrometry (GC−MS), high-performance liquid chromatography (HPLC), HPLC−mass spectrometry (HPLC-MS), etc.[8−10] However, these methods cannot meet the demand of the rapid detection of PCD due to the need for professional operation, expensive instruments, and time-consuming analysis, which limits their application for real-time detection. Compared with large-scale instruments, an immunoassay can be an efficient method due to the advantages of high selectivity and high-throughput detection and it improves the detection efficiency to some extent.[11] Generally, this method for the rapid screening of PCD is applied to qualitative and semiquantitative detection. Immunoassays combined with electrochemical detection have aroused increasing interest because of their fast response time, cost efficiency, and good specificity.[12−15] Nevertheless, the sensitivity and stability of an immunoassay could be limited by the restricted signal amplification strategy[16] and there have been insufficient detection methods for PCD these recent years. Hence, there is an urgent need to design appropriate methods for rapid, sensitive detection of PCD in environmental samples and agricultural products.

Introducing functional materials with remarkable properties into antibodies could improve their sensing performance, which contributes to amplification of sensing signals and further increases the sensitivity of sensors.[17−19] Due to the fascinating optical and electronic properties, gold nanoparticles have been employed in sensing fields,[20,21] which could improve the electron transfer rate as well as capture antibodies.[22,23] In the meantime, macrocyclic compounds are proven to be encouraging candidates for AuNP surface functionalization.[24−26] The introduction of gold composites and macrocycle is expected to be an extensive improvement in the analytical performance of the sensor by providing a higher electron transfer rate as well as more active sites.[27,28] Belonging to a family of supramolecular hosts, β-cyclodextrin (β-CD) has triggered extensive interest owing to its good water solubility, environment-friendly properties, and remarkable molecular recognition performance.[29−31] β-CD possesses a unique inner cavity and can selectively bind molecules to form stable host−guest inclusion complexes, which has been widely utilized in fabricating supramolecular functionalized sensing systems for

Received: November 14, 2024
Revised: December 25, 2024
Accepted: December 27, 2024
Published: January 12, 2025

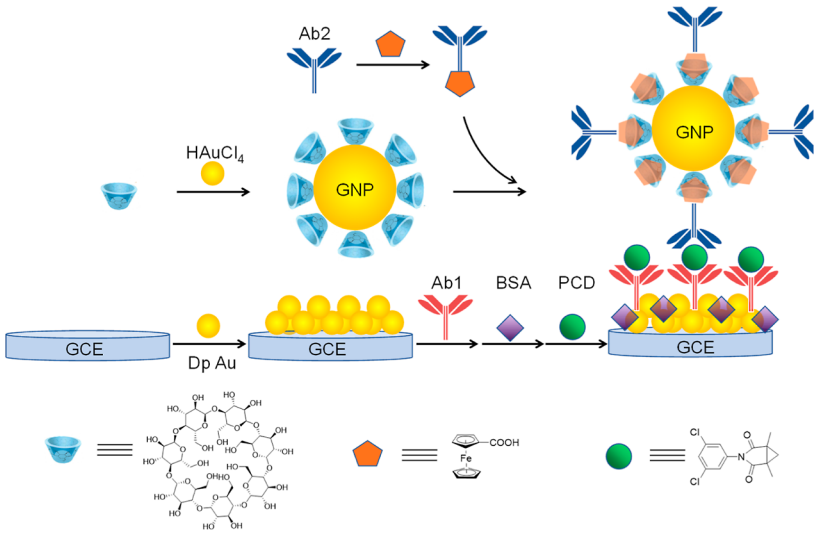

Figure 1. Schematic illustration of the fabrication process of the immunosensor.

the detection of pollutants.[17,32−34] Ferrocene, a well-known redox probe, has been a popular candidate for β-CD to form Fc/β-CD complexes which are employed in electrochemical sensors.[35−37] Shen et al.[38] reported an electrochemical sensor based on host−guest nanonets of Fc−Fc/β-CD/PAMAM-Au catalyzing amplification for procalcitonin detection. Yan et al.[16] employed Fc-β-CD@Fe_3O_4@SiO_2@CDs-MWCNT nanostructures to construct an electrochemical immunosensor for carcino-embryonic antigens. In these previous research studies, Fc derivative-bound β-CD molecules were used as trace labels and contributed to the electrochemical responses. Normally, Fc/β-CD complexes were immobilized on the substrate or formed bioconjugates with the aid of other supporting structures (such as polymer PAMAM or MWCNT in the above work), which might result in complex processes for fabricating sensors.

In this study, a simple sandwich-type electrochemical immunosensor based on a supramolecular amplification strategy was constructed for sensitive detection of PCD. The fabrication process of the immunosensor consisted of the following steps (Figure 1). First, a glass carbon electrode was electrodeposited on gold, followed by immersion of monoclonal antibodies (Ab1). Subsequently, β-CD-capped GNPs were synthesized and introduced to immobilize ferrocene monocarboxylic acid-functionalized antigens (Ab2) based on host−guest interactions. β-CD functional-labeled bioconjugates (FC/β-CD/GNPs−Ab2) were formed. Here, β-CD capped GNPs played the role of carriers for antibodies and electroactive species. FC/β-CD/GNP complexes could provide more sites for Ab2 and increase electroactive species, contributing to improved detection sensitivity and great signal amplification. After that, with the presence of target PCD, β-CD functional-labeled bioconjugates combined with Ab1 to fabricate a sandwich-type immunosensor based on antigen−antibody interactions. The proposed immunosensor was monitored with differential pulse voltammetry. In addition, the stability, specificity, and real sample applications of the sensor were investigated. The proposed immunosensor extended a wide linear range from 5 pM to 0.1 μM, along with a low detection limit (1.67 pM). This work enriches the immunoassay analysis strategy and contributes to the development of rapid, quantitative, and sensitive detection of PCD.

2. MATERIALS AND METHODS

2.1. Reagents and Chemicals. Procymidone (PCD) was purchased from Ehrenstorfer GmbH Co., Ltd. (Augsburg, Germany). Procymidone monoclonal antibodies (Ab1, 6.3 mg/mL) and procymidone a complete antigen (Ab2, 8.5 mg/mL) were obtained from Anti Biological Technology Co., Ltd. (Shenzhen, China). β-Cyclodextrin (β-CD) and ferrocene monocarboxylic acid (Fc−COOH) were purchased from Tokyo Chemical Industry Co., Ltd. (Tokyo, TCI). Chloroauric acid ($HAuCl_4$·$4H_2O$), *N*-(3-(dimethylamino)propyl)-*N*′-ethylcarbodiimide hydrochloride (EDC), *N*-hydroxysuccinimide (NHS), and bovine serum albumin (BSA) were obtained from Sinopharm Chemical Reagent Co., Ltd. (Shanghai, China). Pesticide standards including malathion (MLT), carbofuran (CBF), diflubenzuron (DBZ), profenofos (PFO), and prochloraz (PRO) were purchased from the Agro-Environmental Protection Institute, Ministry of Agriculture and Rural Affairs (Tianjin, China). All reagents and solvents were analytical-reagent-grade and used without further purification. Deionized water from a Milli-Q water purification system was used to prepare all of the solutions (18.2 MΩ).

2.2. Instruments. Cyclic voltammetry (CV), electrochemical impedance spectroscopy (EIS), and differential pulse voltammetry (DPV) measurements were performed with a CHI 660E electrochemical workstation (Chenhua, China). The morphology of the as-prepared particles was measured using a Talos F200X transmission electron microscope (FEI, America). Fourier transform infrared (FTIR) spectra were measured with a Nicolet IS 10 spectrometer (Thermo Fisher, America). UV−vis spectra were collected on a Lambda 35 spectrophotometer (PerkinElmer, America).

2.3. Synthesis of β-CD-Capped GNPs. Gold nanoparticles were prepared by following the reported literature.[39] 15.6 mL of DI water (15.6 mL), 4.0 mL of 10 mM β-CD, and 0.2 mL of 20.3 mM $HAuCl_4$ were first mixed at room temperature. Subsequently, 0.04 mL of 1 M NaOH was added to the above solution with vigorous stirring. Then the reaction mixture was heated in a water bath at 60 °C for 10−15 min. The color of the solution turned to red, indicating the formation of gold nanoparticles.

2.4. Preparation of β-CD Functional-Labeled Bioconjugates (FC/β-CD/GNPs−Ab2). The proposed FC/β-

https://doi.org/10.1021/acsomega.4c10354
ACS Omega 2025, 10, 3108−3115

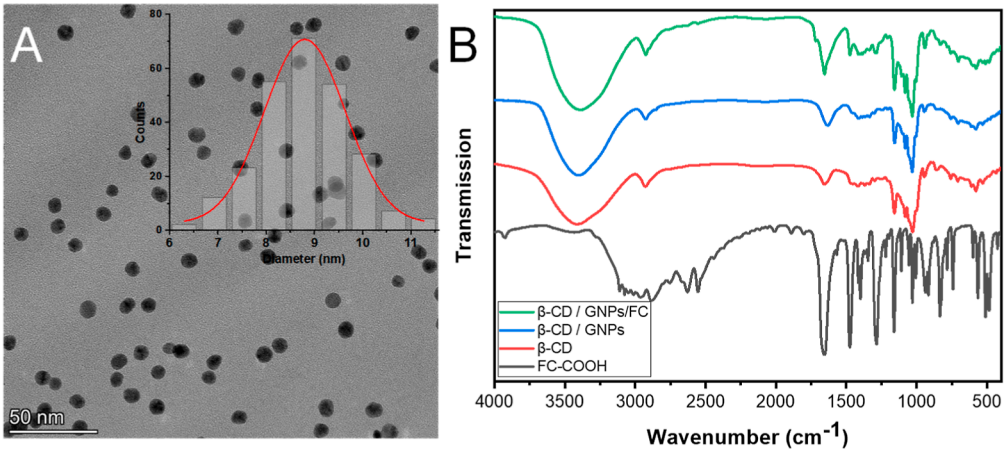

Figure 2. (A) TEM image of β-CD-capped GNPs. The inset shows the size distribution of β-CD/GNPs. (B) FTIR spectra of FC−COOH, β-CD, β-CD/GNPs, and β-CD/GNPs/FC.

CD/GNPs-Ab2 were prepared according to the literature.[38] First, FC−COOH (35 mg) was suspended in 15 mL of DI water with ultrasonication. Then, 10 mg of EDC and 10 mg of NHS were added with continual stirring. The β-CD-capped GNPs were treated with centrifugation at 12,000 rpm for 30 min. The obtained condensed GNPs were mixed with the FC solution described above with the aid of ultrasonication. Subsequently, 100 μL of Ab2 was added into the above mixture for 4 h at 4 °C. Finally, the proposed β-CD functional-labeled bioconjugates were collected by centrifugation, washed with PBS, and stored at −20 °C for further use. For comparison, the FC-labeled Ab2 bioconjugates (FC−Ab2) were prepared with the same procedure without adding the GNP solution.

2.5. Fabrication of the Immunosensor. The fabrication process of the immunosensor is illustrated in Figure 1. First, the GCE was polished with 1.0, 0.3, and 0.05 μm alumina, followed by ultrasonicating it in isopropanol, ethanol, and DI water and drying with nitrogen. Subsequently, electrochemical deposition was carried out in 2 mL of 10 mM $HAuCl_4$ under a potential of −0.2 V for 60 s. The electrode was incubated in 10 μL of Ab1 overnight at 4 °C. Then, 10 μL of a 1 wt % BSA solution was incubated for 60 min to block nonspecific active sites. Next, 10 μL of PCD with different concentrations was added dropwise onto the electrodes and incubated for 1 h at 4 °C. Finally, the sandwich-type immunosensor was fabricated after immobilization of the Ab2-labeled bioconjugate suspension for 1 h at 4 °C. The immunosensor was rinsed with PBS buffer, dried with nitrogen, and stored at 4 °C when not in use.

The performance of the proposed immunosensor was evaluated by the differential pulse voltammetry (DPV) technique with three electrode systems. A platinum wire was used as the counter electrode, and a Ag|AgCl|3 M KCl electrode was used as the reference electrode. The DPV parameters applied were a 50 mV/s sweeping rate, a 60 ms pulse width, a 0.5 s pulse period, and a voltage range from 0.1 to 0.6 V.

2.6. Pretreatment of Real Samples. Chives and cucumbers were purchased from a local supermarket and cleaned with distilled water to remove adsorptive residues from farm sprays. Edible portions of these two vegetables were crushed in vegetable juice. The sample (10 g) was immersed in 10 mL of acetonitrile, followed by the addition of magnesium sulfate (4 g), sodium chloride (1 g), and trisodium citrate dihydrate (0.5 g). Then the mixture was fully placed on a vortex mixer, followed by centrifugation at 4200 rpm for 5 min. Subsequently, the obtained supernatant was mixed with magnesium sulfate (1.5 g), primary secondary amine (PSA, 150 mg), and graphitized carbon black (GCB, 15 mg). The mixture was centrifuged at 4200 rpm for 5 min, followed by filtration (0.22 μm membrane) to remove any suspended particulate materials. The obtained solution was a real sample for future use.

3. RESULTS AND DISCUSSION

3.1. Characterization of β-CD-Capped GNPs and FC/β-CD/GNP Complexes. The morphology of as-prepared β-CD-capped GNPs was determined through TEM. As shown in Figure 2A, the nanoparticles were observed to be well dispersed, with a Gaussian particle size distribution of about 8.8 nm.

FTIR spectroscopy was conducted for structure analysis. Figure 2B displays the FTIR spectra of FC−COOH (black curve), β-CD (red curve), β-CD/GNPs (blue curve), and FC/β-CD/GNPs (green curve). Characteristic vibration peaks of FC−COOH and β-CD are marked with black and red dashed lines, respectively (Figure S1). In the spectrum of FC−COOH, three evident peaks at 1476, 1284, and 1109 cm^{-1} were assigned to the C=O vibration, C−H stretching, and FC ring tilt, respectively. Ferrocene with bands at 836 and 783 cm^{-1} would be expected to be prominent also in the spectrum of the inclusion complex.[40] In the spectrum of β-CD, characteristic absorption peaks at 3400 and 2927 cm^{-1} were attributed to the O−H stretching vibration and C−H stretching, respectively. The characteristic peak at 1081 cm^{-1} was assigned to the C−C bending vibration.[41] Several major peaks of FC/β-CD/GNPs complexes were consistent with β-CD and FC−COOH. The decrease of the absorption peaks of the functional groups of guest molecules in the FTIR spectrum of FC/β-CD/GNPs was observed, indicating the encapsulation of FC−COOH inside the β-CD cavity and conformation of the formation of the complexes.

Furthermore, the interactions between FC−COOH and β-CD functional materials were investigated with UV−vis measurement. As illustrated in Figure S2, FC−COOH showed a characteristic absorption peak at 445 nm (red curve). The absorption peak of FC−COOH was observed to be blue-shifted to 440 nm (blue curve) after the addition of β-CD/

https://doi.org/10.1021/acsomega.4c10354
ACS Omega 2025, 10, 3108−3115

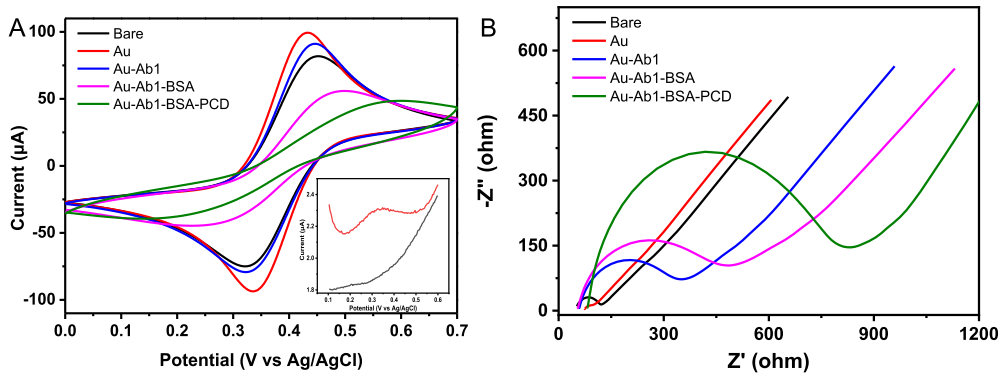

Figure 3. Cyclic voltammetry (A) and electrochemical impedance spectroscopy (B) of different modified electrodes in KCl, containing 5.0 mM $[Fe(CN)_6]^{3-/4-}$ as the redox probe. The inset shows the DPV curve of the modified electrode (Au−Ab1−BSA−PCD) before (black curve) and after (red curve) assembly of Ab2 bioconjugates.

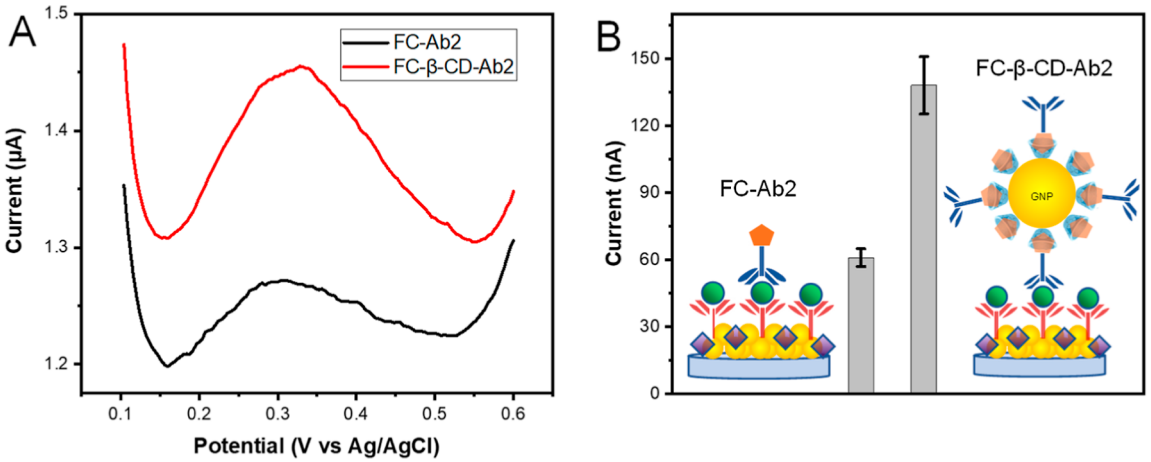

Figure 4. Differential pulse voltammetry (A) and the histogramed peak current (B) of immunosensors with different labeled Ab2 bioconjugates.

GNPs, implying the interaction between FC−COOH and β-CD/GNPs. A distinct absorption peak at 520 nm (marked with a green arrow in the black curve) was attributed to β-CD/GNPs, which displayed a decreased intensity after interaction with FC−COOH (blue curve).

3.2. Electrochemical Characterization of the Immunosensor. Cyclic voltammetry (CV) and electrochemical impedance spectroscopy (EIS) measurements were carried out to monitor the modification of the electrode in the presence of 5 mM $[Fe(CN)_6]^{3-/4-}$ as a redox probe in 0.1 M KCl (Figure 3). As shown in Figure 3A, the bare GCE showed a pair of well-defined redox peaks (black curve). An increased current was observed after electrodeposition of gold because of the larger electron transfer to the electrode surface (red curve). Subsequently, the redox current decreased attributed to the hindering effect with the assembly of Ab1 (blue curve). BSA could block the nonspecific binding sites, resulting in a further decrease of the redox current (pink curve). In addition, the introduction of PCD could also inhibit electron transfer to the electrode due to the binding between PCD and the antibody Ab1. The peak currents were with an apparent decrease (green curve). DPV measurements were conducted in a PBS buffer without any redox probe. As illustrated in the inset of Figure 3A, a typical DPV peak was obtained after the modification of Ab2 conjunctions. The occurrence of peak current ascribed to the FC group of the β-CD-labeled Ab2 bioconjugates provided strong evidence of the successful fabrication of the sandwich-type immunosensor.

EIS is also a valuable method to characterize the interface properties of the surface-modified electrodes. Figure 3B illustrates that the bare GCE had a small semicircle diameter, suggesting a small electron transfer resistance (R_{ct}) of the electrode (black curve). With the electrodeposition of gold, a distinct decrease of the semicircle was observed (red curve), indicating a lower impedance because of the improved electron transfer process on the gold-modified surface. However, the introduction of antibody Ab1 contributed to increasing R_{ct} because the nonconducting antibody inhibited electron transfer (blue curve). Also, a larger semicircle was observed after the modification of BSA, indicating increased R_{ct} in nonspecific blocked areas (pink curve). Moreover, the immobilization of PCD further increased the R_{ct} value (green curve). These results were consistent with CV measurements, suggesting the successful preparation of Au/Ab1/BSA/PCD/GCE.

3.3. Amplification Properties of β-CD Functional Conjugates. To investigate the amplification properties of β-CD functional-labeled bioconjugates (FC/β-CD−Ab2), FC−COOH-labeled Ab2 bioconjugates (FC−Ab2) were also prepared and used as the contrast project. Figure 4A shows differential pulse voltammetry responses of immunosensors with different labeled Ab2 bioconjugates. As illustrated in Figure 4B, the immunosensor assembled with FC/β-CD−Ab2-

https://doi.org/10.1021/acsomega.4c10354
ACS Omega 2025, 10, 3108−3115

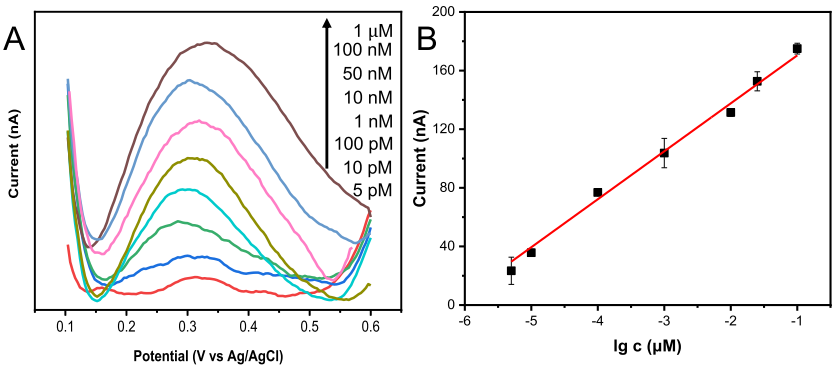

Figure 5. DPV responses (A) and calibration curve (B) of prepared immunosensors with PCD at different concentrations.

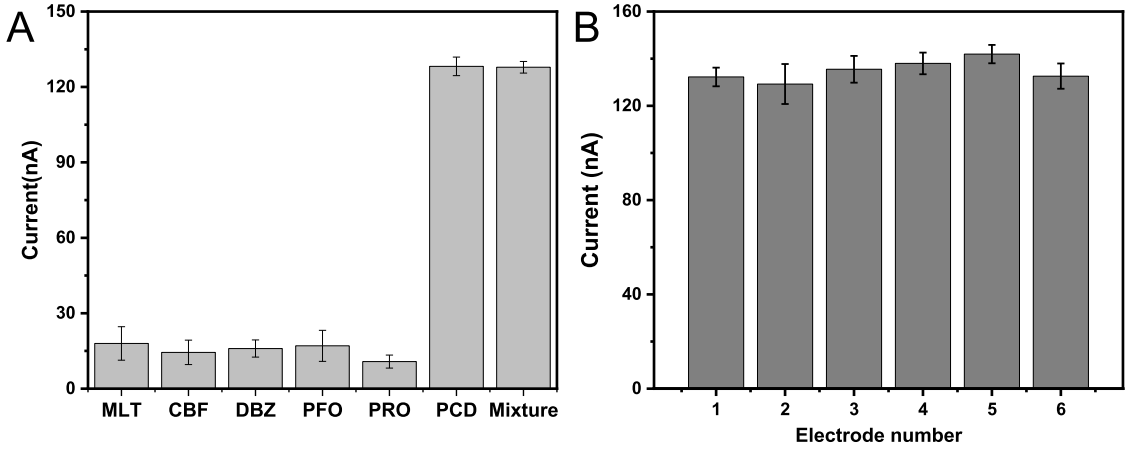

Figure 6. (A) Selectivity of the DPV responses; (B) responsivity of the prepared immunosensor.

labeled bioconjugates (right) displayed over twice larger peak current than those with FC−Ab2-labeled bioconjugates (left), suggesting that β-CD functional bioconjugates owned the advantage of signal amplification. For the β-CD molecules on the surface of gold nanoparticles, β-CD not only played the role of a capping agent but also provided cavities for FC based on host−guest interactions. Thanks to the structure of β-CD-capped GNPs, β-CD functional bioconjugates could afford more electroactive groups. Therefore, β-CD functional materials could contribute to improving electron transfer, which led to a higher responsive signal from the redox mediator and the increased current.

3.4. Optimization of Experimental Conditions. To obtain the best performance of the proposed immunosensor, several key parameters were investigated such as concentration of antibody Ab1, concentration of bioconjugates, incubation time, and pH of the detection solution (Figure S3). The optimization experiments were performed by monitoring the peak current with DPV measurement.

First, the effect of antibody Ab1 concentration was examined over the range from 2 to 40 μg/mL. As shown in Figure S3A, the current value first increased with the increasing concentration of antibody Ab1, and it reached equilibrium around 10 μg/mL. Thus, the Ab1 incubation concentration of 10 μg/mL was selected in the following experiments.

The concentration of β-CD-labeled Ab2 bioconjugates was a key parameter influencing the formation of the sandwich structure, which further affected the response of the immunosensor. Figure S3B displays the current response of the immunosensor incubated with different concentrations of β-CD functional bioconjugates. The peak current increased at the beginning and then tended to a constant while the concentration was at 0.7 mg/mL. This was due to that the increased bioconjugate concentration provided more redox probes for signal generation. Then, the binding between the antibody and the target reached saturation. Therefore, the optimum β-CD-labeled Ab2 bioconjugates' concentration was 0.7 mg/mL.

The incubation time of β-CD-labeled Ab2 bioconjugates was also studied (Figure S3C). It was observed that the current response increased over the incubation time from 10 to 60 min. The increasing incubation time enabled enough bioconjugates to immobilize the electrode to form a sandwich-type immunosensor. Then, the current tended to be stable when the incubation time was over 60 min, indicating the saturated interaction between the antibody and antigen. As a result, 60 min was chosen as the incubation time for the detection experiments.

The response signal of the electrochemical immunosensor was influenced by the pH of the solution. pH dependence of voltammetry response was investigated (Figure S3D). With the pH increasing from 5.0 to 8.0, the peak current increased first and decreased when the pH was over 7.0. The current value reached a maximum at 7.0 eV, indicating the best performance of the immunosensor. Consequently, pH 7.0 was employed as the optimal pH value in the subsequent electrochemical measurements.

3.5. Detection of Procymidone Based on the Sandwich-Type Immunosensor. Under the optimum conditions, the proposed immunosensor was employed to

https://doi.org/10.1021/acsomega.4c10354
ACS Omega 2025, 10, 3108−3115

detect PCD with the DPV technique. Figure 5A illustrates the DPV responses of the immunosensors with PCD at various concentrations. The current signal was observed to gradually increase with the increasing concentration of PCD. The peak current values versus PCD concentration from 5 pM to 1 μM were recorded. As shown in Figure 5B, the peak current (Ip) showed a good linear relationship with the logarithm of PCD concentration (lgc) in the range from 5 pM to 0.1 μM. The linear equation Ip (nA) = $2.03 \times 10^{-7} + 3.32 \times 10^{-8}$*lgc($\mu$M), with R^2 = 0.992. The LOD of the proposed method was calculated at 1.67 pM according to 3 times the standard deviation of the blank,[42,43] which was far lower than the maximum level for vegetables (7.02 μM, 2 mg/kg) permitted by the Chinese National Standard. In addition, the proposed method was found to be comparable with reported sensors with a lower detection limit (Table S1).

3.6. Selectivity, Stability, and Reproducibility of the Prepared Immunosensor. For the practical application of immunosensors, binding selectivity between antigens and antibodies plays a significant role.[44,45] A selectivity experiment was conducted, including some possible interferents such as MLT, CBF, DBZ, PFO, and PRO (Figure 6A). The chemical structures of pesticides in this project are shown in Figure S4. DPV responses of the prepared sensor were recorded by incubation in the following samples under the same condition, where the concentration of the molecules was 5 ng/mL (the corresponding molar concentration for PCD was 17.6 nM). It was found that only the immunosensor incubated with PCD displayed a significant current response. In addition, the current of the immunosensor incubated with the mixture containing PCD and other interfering species presented an inconspicuous difference compared with that of PCD. These results demonstrated the excellent selectivity of the proposed immunosensor.

An assessment of stability was performed by the analysis of the same concentration of PCD with three prepared electrodes. Figure S5 shows the DPV responses of the sensors within 4 weeks. After 4 weeks, the current responses of the immunosensors were retained at no less than 82% of the initial response. Furthermore, the reproducibility of PCD was estimated toward six sensors that were prepared independently (Figure 6B). The RSD was found as 3.1%. Therefore, the prepared immunosensor exhibited good stability and reproducibility to PCD.

3.7. Determination of Procymidone in Real Samples. For the potential application in real samples, the proposed immunosensor was examined using chives and cucumber samples. Recovery experiments were performed with the PCD concentrations of 0.35, 1.75, and 3.50 nM. As illustrated in Table 1, the proposed immunosensor produced an acceptable return percentage from 92.2% to 105.1%. Furthermore, the real samples were analyzed using the HPLC-MS method (Table S2). Notably, the detection results from the electrochemical method were in agreement with those obtained by the HPLC-MS method, indicating the good and acceptable reliability as well as applicability of the proposed method to real samples.

Table 1. Detection of PCD in Chives and Cucumber Samples

samples	added (nM)	found (nM)	RSD (%, n = 3)	recovery (%)
Chives	0.00	0.196	1.70	
	0.35	0.351	1.23	100.3
	1.75	1.690	5.19	96.6
	3.50	3.228	3.73	92.2
Cucumbers	0.00	0.022	1.86	
	0.35	0.368	3.29	105.1
	1.75	1.640	6.92	93.7
	3.50	3.610	1.91	103.1

4. CONCLUSIONS

In summary, we developed a sandwich-type electrochemical immunosensor for procymidone detection based on the FC/β-CD host–guest supramolecular system. The multiplex labeling of electroactive FC on the β-CD functional bioconjugates was implemented by host–guest interactions, which greatly contributed to the signal amplification. The fabricated sensor exhibited remarkable electrochemical activity toward procymidone with a wide linear range and a low detection limit of 5 pM–0.1 μM and 1.67 pM, respectively. Moreover, the supramolecular sensing system displayed satisfactory analytical performances in terms of high sensitivity, excellent selectivity, and good stability as well as a prominent ability to detect procymidone in complex matrixes. This work provides a simple and useful tool for the fast determination of procymidone. In view of all of these features, we can conclude that our work can be expanded for procymidone monitoring.

■ ASSOCIATED CONTENT

Supporting Information

The Supporting Information is available free of charge at https://pubs.acs.org/doi/10.1021/acsomega.4c10354.

Zoomed FTIR spectra corresponding to Figure 2B; UV–vis spectroscopy of β-CD/GNPs, FC–COOH, and β-CD/GNPs/FC; optimization of experimental parameters; chemical structures of pesticides; DPV responses of the prepared immunosensors at different storage days; comparison of different methods of detecting PCD; and detection of PCD in chives and cucumber samples by the HPLC-MS method (PDF)

■ AUTHOR INFORMATION

Corresponding Authors

Dawen Zhang − *Key Laboratory for Quality and Safety Control of Poultry Products, Ministry of Agriculture and Rural Affairs of the People's Republic of China, Institute for Quality & Safety and Standards of Agricultural Products Research, Jiangxi Academy of Agricultural Sciences, Nanchang, Jiangxi 330200, China*; Email: zdw3296@163.com

Suyan Qiu − *Key Laboratory for Quality and Safety Control of Poultry Products, Ministry of Agriculture and Rural Affairs of the People's Republic of China, Institute for Quality & Safety and Standards of Agricultural Products Research, Jiangxi Academy of Agricultural Sciences, Nanchang, Jiangxi 330200, China*; orcid.org/0000-0002-2708-8722; Email: qiusuyan@126.com

Authors

Qiushuang Ai − *Key Laboratory for Quality and Safety Control of Poultry Products, Ministry of Agriculture and Rural Affairs of the People's Republic of China, Institute for Quality & Safety and Standards of Agricultural Products Research, Jiangxi Academy of Agricultural Sciences, Nanchang, Jiangxi 330200, China*; orcid.org/0009-0009-0629-631X

https://doi.org/10.1021/acsomega.4c10354
ACS Omega 2025, 10, 3108−3115

Xiren Yu − *Key Laboratory for Quality and Safety Control of Poultry Products, Ministry of Agriculture and Rural Affairs of the People's Republic of China, Institute for Quality & Safety and Standards of Agricultural Products Research, Jiangxi Academy of Agricultural Sciences, Nanchang, Jiangxi 330200, China*

Yifan Dong − *Key Laboratory for Quality and Safety Control of Poultry Products, Ministry of Agriculture and Rural Affairs of the People's Republic of China, Institute for Quality & Safety and Standards of Agricultural Products Research, Jiangxi Academy of Agricultural Sciences, Nanchang, Jiangxi 330200, China*

Li Zhang − *Key Laboratory for Quality and Safety Control of Poultry Products, Ministry of Agriculture and Rural Affairs of the People's Republic of China, Institute for Quality & Safety and Standards of Agricultural Products Research, Jiangxi Academy of Agricultural Sciences, Nanchang, Jiangxi 330200, China*

Jingtian Liang − *Key Laboratory for Quality and Safety Control of Poultry Products, Ministry of Agriculture and Rural Affairs of the People's Republic of China, Institute for Quality & Safety and Standards of Agricultural Products Research, Jiangxi Academy of Agricultural Sciences, Nanchang, Jiangxi 330200, China*

Complete contact information is available at: https://pubs.acs.org/10.1021/acsomega.4c10354

Notes

The authors declare no competing financial interest.

■ ACKNOWLEDGMENTS

This study was financially supported by the Natural Science Foundation of Jiangxi Province of China (No. 20232BAB215020) and Jiangxi Special Fund for Agro-scientific Research in the Collaborative Innovation (No. JXXTCXBSJJ202211 and No. JXXTCX202110).

■ REFERENCES

(1) Lin, S.; Han, Y.; Jiangyuan, C.; Luo, Y.; Xu, W.; Luo, H.; Pang, G. Revealing the biodiversity and the response of pathogen to a combined use of procymidone and thiamethoxam in tomatoes. *Food Chem.* **2019**, *284*, 73−79.

(2) Zhang, S.; Li, L.; Meng, G.; Zhang, X.; Hou, L.; Hua, X.; Wang, M. Environmental behaviors of procymidone in different types of chinese soil. *Sustainability* **2021**, *13*, 6712.

(3) Li, Y.; Qin, G.; He, F.; Zou, K.; Zuo, B.; Liu, R.; Zhang, W.; Yang, B.; Zhao, G.; Jia, G. Investigation and analysis of pesticide residues in edible fungi produced in the mid-western region of china. *Food Control* **2022**, *136*, 108857.

(4) Abe, J.; Tomigahara, Y.; Tarui, H.; Omori, R.; Kawamura, S. Identification of metabolism and excretion differences of procymidone between rats and humans using chimeric mice: Implications for differential developmental toxicity. *J. Agric. Food Chem.* **2018**, *66*, 1955−1963.

(5) Lai, Q.; Sun, X.; Li, L.; Li, D.; Wang, M.; Shi, H. Toxicity effects of procymidone, iprodione and their metabolite of 3, 5-dichloroaniline to zebrafish. *Chemosphere* **2021**, *272*, 129577.

(6) Tarui, H.; Tomigahara, Y.; Nagahori, H.; Sugimoto, K.; Mogi, M.; Kawamura, S.; Isobe, N.; Kaneko, H. Species differences in the developmental toxicity of procymidone-placental transfer of procymidone in pregnant rats, rabbits, and monkeys. *J. Pestic. Sci.* **2018**, *43*, 79−87.

(7) Wu, A.; Yu, Q.; Lu, H.; Lou, Z.; Zhao, Y.; Luo, T.; Fu, Z.; Jin, Y. Developmental toxicity of procymidone to larval zebrafish based on physiological and transcriptomic analysis. *Comp. Biochem. Physiol., Part C: Toxicol. Pharmacol.* **2021**, *248*, 109081.

(8) Chu, Y.; Tong, Z.; Dong, X.; Sun, M.; Gao, T.; Duan, J.; Wang, M. Simultaneous determination of 98 pesticide residues in strawberries using UPLC-MS/MS and GC-MS/MS. *Microchem. J.* **2020**, *156*, 104975.

(9) Duan, Y.; Li, Y.; Liu, J. Determination of procymidone residues in panax notoginseng by gas chromatography-tandem mass spectrometry. *J. Food Saf. Food Qual.* **2018**, *9*, 5716−5720.

(10) Özdoğan, N.; Kapukıran, F.; Mutluoğlu, G.; Chormey, D. S.; Bakırdere, S. Simultaneous determination of iprodione, procymidone, and chlorflurenol in lake water and wastewater matrices by GC-MS after multivariate optimization of binary dispersive liquid-liquid microextraction. *Environ. Monit. Assess.* **2018**, *190*, 1−7.

(11) Chen, Z.; He, X.; Huang, S.; Liu, J.; Chen, Y.; Wang, H.; Xiao, Z.; Xu, Z.; Xu, M. Rapid detection of procymidone in vegetables by nanobody-based colloidal gold immunochromatography assay. *Food Sci.* **2022**, *43*, 1−14.

(12) Wang, J.; Chen, F.; Yang, Q.; Meng, Y.; Jiang, M.; Wang, Y.; Zhang, D.; Du, L. Light-addressable electrochemical immunoassay for multiplexed detection of antigen. *Sens. Actuators, B* **2023**, *374*, 132821.

(13) Dai, L.; Xu, R.; Cui, M.; Ren, X.; Wang, X.; Feng, J.; Wu, R.; Ma, H.; Wei, Q. A high throughput dual-signal ultra-sensitive electrochemical and photoelectrochemical microfluidic immunoassay platform with raspberry Au/PANI@ CdS for Cyfra 21−1 detection. *Biosens. Bioelectron.: X* **2022**, *11*, 100207.

(14) Osaki, S.; Espulgar, W. V.; Wakida, S.; Saito, M.; Tamiya, E. Optimization of electrochemical analysis for signal amplification in gold nanoparticle-probed immunoassays. *Electrochim. Acta* **2022**, *432*, 141180.

(15) Dorozhko, E.; Kazachinskaia, E.; Kononova, Y.; Zaikovskaya, A.; Barek, J.; Korotkova, E.; Kolobova, E.; Sheveleva, P.; Saqib, M. Electrochemical immunoassay of antibodies using freshly prepared and aged conjugates of silver nanoparticles. *Talanta* **2023**, *253*, 124028.

(16) Yan, Z.; Ma, H.; Fan, D.; Hu, L.; Pang, X.; Gao, J.; Wei, Q.; Wang, Q. An ultrasensitive sandwich-type electrochemical immunosensor for carcino embryonie antigen based on supermolecular labeling strategy. *J. Electroanal. Chem.* **2016**, *781*, 289−295.

(17) Mei, X.; Wang, X.; Huang, W.; Zhu, J.; Liu, K.; Wang, X.; Cai, W.; He, R. A novel polycaprolactone/polypyrrole/β-cyclodextrin electrochemical flexible sensor for dinotefuran pesticide detection. *Food Chem.* **2024**, *434*, 137194.

(18) Wang, Y.; Zeng, R.; Tian, S.; Chen, S.; Bi, Z.; Tang, D.; Knopp, D. Bimetallic single-atom nanozyme-based electrochemical-photothermal dual-function portable immunoassay with smartphone imaging. *Anal. Chem.* **2024**, *96*, 13663−13671.

(19) Wu, D.; Tang, J.; Yu, Z.; Gao, Y.; Zeng, Y.; Tang, D.; Liu, X. Pt/Zn-TCPP nanozyme-based flexible immunoassay for dual-mode pressure-temperature monitoring of low-abundance proteins. *Anal. Chem.* **2024**, *96*, 8740−8746.

(20) Rahimizadeh, K.; Zahra, Q.; Chen, S.; Le, B. T.; Ullah, I.; Veedu, R. N. Nanoparticles-assisted aptamer biosensing for the detection of environmental pathogens. *Environ. Res.* **2023**, *238*, 117123.

(21) Pechyen, C.; Tangnorawich, B.; Toommee, S.; Marks, R.; Parcharoen, Y. Green synthesis of metal nanoparticles, characterization, and biosensing applications. *Sens., Int.* **2024**, *5*, 100287.

(22) Xu, J.; Zhang, J.; Zeng, R.; Li, L.; Li, M.; Tang, D. Target-induced photocurrent-polarity-switching photoelectrochemical aptasensor with gold nanoparticle- $ZnIn_2S_4$ nanohybrids for the quantification of 8-hydroxy-2′-deoxyguanosine. *Sens. Actuators, B* **2022**, *368*, 132141.

(23) Cai, G.; Yu, Z.; Ren, R.; Tang, D. Exciton-plasmon interaction between aunps/graphene nanohybrids and CdS quantum dots/TiO_2 for photoelectrochemical aptasensing of prostate-specific antigen. *ACS Sens* **2018**, *3*, 632−639.

(24) Ai, Q.; Jin, L.; Gong, Z.; Liang, F. Observing host-guest interactions at molecular interfaces by monitoring the electrochemical current. *ACS Omega* **2020**, *5*, 10581−10585.
(25) Ma, T.; Chang, S.; He, J.; Liang, F. Emerging sensing platforms based on cucurbit[n]uril functionalized gold nanoparticles and electrodes. *Chem. Commun.* **2023**, *60*, 150−167.
(26) Zhao, Y.; Huang, Y.; Zhu, H.; Zhu, Q.; Xia, Y. Three-in-one: Sensing, self-assembly, and cascade catalysis of cyclodextrin modified gold nanoparticles. *J. Am. Chem. Soc.* **2016**, *138*, 16645−16654.
(27) Li, J.; Hu, X.; Zhou, Y.; Zhang, L.; Ge, Z.; Wang, X.; Xu, W. β-cyclodextrin-stabilized Au nanoparticles for the detection of butyl benzyl phthalate. *ACS Appl. Nano Mater.* **2019**, *2*, 2743−2751.
(28) Sahu, B.; Kurrey, R.; Deb, M. K.; Khalkho, B. R.; Manikpuri, S. Recognition of malathion pesticides in agricultural samples by using α-CD functionalized gold nanoparticles as a colorimetric sensor. *Talanta* **2023**, *259*, 124526.
(29) Guo, J.; Hou, J.; Hu, J.; Geng, Y.; Li, M.; Wang, H.; Wang, J.; Luo, Q. Recent advances in β-cyclodextrin-based materials for chiral recognition. *Chem. Commun.* **2023**, *59*, 9157−9166.
(30) Kou, X.; Gao, N.; Xu, X.; Zhu, J.; Ke, Q.; Meng, Q. Preparation, structural analysis of alcohol aroma compounds/β-cyclodextrin inclusion complexes and the application in strawberry preservation. *Food Chem.* **2024**, *457*, 140160.
(31) He, Y.; Zheng, Y.; Liu, C.; Zhang, H.; Shen, J. Citric acid cross-linked β-cyclodextrins: A review of preparation and environmental/biomedical application. *Carbohydr. Polym.* **2024**, *323*, 121438.
(32) Liu, Y.; Liu, Y.; Liu, Z.; Du, F.; Qin, G.; Li, G.; Hu, X.; Xu, Z.; Cai, Z. Supramolecularly imprinted polymeric solid phase microextraction coatings for synergetic recognition nitrophenols and bisphenol a. *J. Hazard. Mater.* **2019**, *368*, 358−364.
(33) Tu, X.; Gao, F.; Ma, X.; Zou, J.; Yu, Y.; Li, M.; Qu, F.; Huang, X.; Lu, L. Mxene/carbon nanohorn/β-cyclodextrin-Metal-organic frameworks as high-performance electrochemical sensing platform for sensitive detection of carbendazim pesticide. *J. Hazard. Mater.* **2020**, *396*, 122776.
(34) Zhang, Y.; Qi, X.; Zhang, X.; Huang, Y.; Ma, Q.; Guo, X.; Wu, Y. β-cyclodextrin/carbon dots-grafted cellulose nanofibrils hydrogel for enhanced adsorption and fluorescence detection of levofloxacin. *Carbohydr. Polym.* **2024**, *340*, 122306.
(35) Ning, S.; Zhou, M.; Liu, C.; Waterhouse, G. I. N.; Dong, J.; Ai, S. Ultrasensitive electrochemical immunosensor for avian leukosis virus detection based on a β-cyclodextrin-nanogold-ferrocene host-guest label for signal amplification. *Anal. Chim. Acta* **2019**, *1062*, 87−93.
(36) Niu, X.; Yang, X.; Mo, Z.; Guo, R.; Liu, N.; Zhao, P.; Liu, Z.; Ouyang, M. Voltammetric enantiomeric differentiation of tryptophan by using multiwalled carbon nanotubes functionalized with ferrocene and β-cyclodextrin. *Electrochim. Acta* **2019**, *297*, 650−659.
(37) Xie, X.; Wang, H.; Zhang, L.; Liu, Y.; Chai, Y.; Yuan, Y.; Yuan, R. A novel electrochemiluminescence immunosensor based on functional β-cyclodextrin-ferrocene host-guest complex with multiple signal amplification. *Sens. Actuators, B* **2018**, *258*, 1146−1151.
(38) Shen, W.; Zhuo, Y.; Chai, Y.; Yang, Z.; Han, J.; Yuan, R. Enzyme-free electrochemical immunosensor based on host-guest nanonets catalyzing amplification for procalcitonin detection. *ACS Appl. Mater. Interfaces* **2015**, *7*, 4127−4134.
(39) Huang, T.; Meng, F.; Qi, L. Facile synthesis and one-dimensional assembly of cyclodextrin-capped gold nanoparticles and their applications in catalysis and surface-enhanced raman scattering. *J. Phys. Chem. C* **2009**, *113*, 13636−13642.
(40) Heise, H. M.; Kuckuk, R.; Bereck, A.; Riegel, D. Infrared spectroscopy and raman spectroscopy of cyclodextrin derivatives and their ferrocene inclusion complexes. *Vib. Spectrosc.* **2010**, *53*, 19−23.
(41) Xiao, Z.; Yu, P.; Sun, P.; Kang, Y.; Niu, Y.; She, Y.; Zhao, D. Inclusion complexes of β-cyclodextrin with isomeric ester aroma compounds: Preparation, characterization, mechanism study, and controlled release. *Carbohydr. Polym.* **2024**, *333*, 121977.
(42) Zeng, R.; Qiu, M.; Wan, Q.; Huang, Z.; Liu, X.; Tang, D.; Knopp, D. Smartphone-based electrochemical immunoassay for point-of-care detection of SARS-COV-2 nucleocapsid protein. *Anal. Chem.* **2022**, *94*, 15155−15161.
(43) Yu, Z.; Qiu, C.; Huang, L.; Gao, Y.; Tang, D. Micro-electromechanical microsystems-supported photothermal immunoassay for point-of-care testing of aflatoxin B1 in foodstuff. *Anal. Chem.* **2023**, *95*, 4212−4219.
(44) Yu, Z.; Gong, H.; Xu, J.; Li, Y.; Xue, F.; Zeng, Y.; Liu, X.; Tang, D. Liposome-embedded $Cu_{2-x}Ag_xS$ nanoparticle-mediated photothermal immunoassay for daily monitoring of ctni protein using a portable thermal imager. *Anal. Chem.* **2022**, *94*, 7408−7416.
(45) Gao, Y.; Li, M.; Zeng, Y.; Liu, X.; Tang, D. Tunable competitive absorption-induced signal-on photoelectrochemical immunoassay for cardiac troponin I based on Z-scheme metal-organic framework heterojunctions. *Anal. Chem.* **2022**, *94*, 13582−13589.

https://doi.org/10.1021/acsomega.4c10354
ACS Omega 2025, 10, 3108−3115